Addendum to Proposal P36
Measurement of $\Gamma(K^+ \to e^+\nu)/\Gamma(K^+ \to \mu^+\nu)$
and
Search for heavy sterile neutrinos
using
the TREK detector system

P36 collaboration

January 7, 2011

Abstract

In this report, we will present new progress on the original P36 proposal. Refinement and reconsideration of the systematic uncertainty estimations in the $R_K = \Gamma(K^+ \to e^+\nu)/\Gamma(K^+ \to \mu^+\nu)$ measurement are done. The R_K uncertainties are estimated by grouping them into three categories: (1) imperfect reproducibility of the experimental conditions by a Monte Carlo simulation, (2) performance of particle identification, and (3) background contamination. The systematic uncertainty is obtained by adding each item in quadrature to be $\Delta R_K/R_K = 0.13\%$. In the heavy neutrino (N) search, the experimental sensitivity of the $K^+ \to \mu^+N$ decay is reconfirmed to be $\mathrm{Br}(K^+ \to \mu^+N) \sim 10^{-8}$. The theoretical calculation of the muon polarization is obtained using the masses of the kaon, muon, and heavy neutrino. We successfully observed high quality beam in the J-PARC K1.1BR beamline tuning. Also, we performed a test experiment for an aerogel Cherenkov (AC) counter and found a good performance as an e^+ trigger.

1 Introduction

In the 10th J-PARC PAC, the approval of the P36 proposal was deferred and the P36 collaboration was requested to study more completely the systematic uncertainties in the measurement of $R_K = \Gamma(K^+ \to e^+\nu)/\Gamma(K^+ \to \mu^+\nu)$ and the polarization technique in the heavy neutrino search (N). We present our further studies of P36 since PAC 10, addressing the questions raised in PAC 10. In section 2, estimations of the systematic uncertainties for the R_K measurement will be described. In section 3,

the treatment of the muon polarization in the P36 experiment will be described. Also the theoretical calculation of the muon polarization in $K^+ \to \mu^+ N$ will be explained. The results of the J-PARC K1.1BR beam tuning and the aerogel Cherenkov counter test for an e^+ trigger will be described in sections 4 and 5, respectively.

2 Detailed analysis of systematic uncertainties for the lepton universality experiment

2.1 Error reduction mechanism and possible error contributions in the R_K measurement

2.1.1 Reduction mechanism of systematic uncertainty

Before starting with the details of the uncertainty estimation, we would like to describe the general method for the error reduction mechanism in our R_K measurement. This experiment will be performed employing a stopped K^+ beam in conjunction with a 12-sector iron-core superconducting toroidal spectrometer. Although the detector system is different from NA62 [1] and KLOE [2], we have learned several points from these experiments, which have already achieved quite high suppression of systematic errors. The schematic cross sectional side- and end- views of the detector system are shown in Fig. 1. The R_K ratio is derived from the number of the accepted K_{e2} and $K_{\mu 2}$ events by correcting for the detector acceptance. The R_K value can be determined using the following ratio,

$$R_K = N(\tilde{K}_{e2})/N(\tilde{K}_{\mu 2}) \cdot \Omega(\tilde{K}_{\mu 2})/\Omega(\tilde{K}_{e2}), \quad (1)$$

$$= N(\tilde{K}_{e2})/N(\tilde{K}_{\mu 2}) \cdot N(\tilde{K}_{\mu 2})^{\mathrm{MC}}/N(\tilde{K}_{e2})^{\mathrm{MC}}, \quad (2)$$

where $N(\tilde{K}_{l2})$ denotes the number of radiative corrected $N(\tilde{K}_{l2}) = N(K_{l2}) + N(K_{l2\gamma})$ events, and $N(K_{l2})$ and $N(K_{l2\gamma})$ denote the number of obtained events from the K_{l2} and $K_{l2\gamma}$ decays, respectively. $N(\tilde{K}_{e2})^{\mathrm{MC}}$ and $N(\tilde{K}_{\mu 2})^{\mathrm{MC}}$ are the numbers of accepted events in the simulation for $\tilde{K}_{e2}$ and $\tilde{K}_{\mu 2}$, respectively. Since the K_{e2} and $K_{\mu 2}$ events are measured simultaneously except for the particle identification, the ambiguity of the number of stopped kaon does not contribute to a systematic uncertainty. We do not need to take into account any effects from K^+ intensity fluctuations during data accumulation. As indicated by this form, the general methodology for the reduction of uncertainties in the proposed experiment can be summarized as follows.

- **The R_K measurement using a stopped K^+ beam.**
  The kaon beam history such as beam momentum, emittance, etc, does not contribute to the systematic error because the P36 experiment will be performed using a stopped K^+ beam.

- **Good kinematical resolution for K_{e2} and $K_{\mu 2}$ decays.**
  The kinematical resolution of the K_{e2} and $K_{\mu 2}$ decays is very good because

charged particles from the K^+ decay at rest are detected. A momentum resolution of $\sigma_p = 1$ MeV/c is expected, which is good enough to separate the two decays by momentum analysis.

- **Cancellation mechanism of detector misalignment.**
  The acceptance distortion associated with a misalignment of the K^+ stopper can be eliminated due to the rotational symmetry of the toroidal spectrometer by integrating over all e^+ and μ^+ directions. Also, effects from an asymmetric K^+ stopping distribution are reduced for the same reason.

- **Cancellation mechanism between K_{e2} and $K_{\mu 2}$.**
  Since we form the ratio of the calculated acceptance of K_{e2} and $K_{\mu 2}$ decays at rest, the similarity of the K_{e2} and $K_{\mu 2}$ kinematics reduces the systematic uncertainty due to the imperfect reproducibility of the experimental conditions in the simulation.

- **Position of the Cherenkov counter for the e^+/μ^+ identification.**
  Since we employ the stopped K^+ method, we can put a Cherenkov counter for the e^+/μ^+ identification close to the K^+ decay position. $K_{\mu 2}$ decays with in-flight-decay μ^+s can be rejected effectively.

2.1.2 Systematic uncertainties in the $\Gamma(K^+ \to e^+\nu)/\Gamma(K^+ \to \mu^+\nu)$ measurement

Thus, most of the systematic effects are reduced by forming the ratio of the number of the accepted K_{e2} and $K_{\mu 2}$ events and their acceptances. However, several items will not be cancelled out perfectly, which introduces a systematic error in the R_K measurement. The dominant contributions can be grouped into 3 categories: systematic uncertainty due to (1) misunderstanding of the detector acceptances, (2) PID performance, and (3) background contaminations, as follows:

(1) Misunderstanding of the detector acceptances.

- Events with e^+ momentum lower than the K_{e3} endpoint due to high energy bremsstrahlung generation cannot be used, and the detector acceptance has to be corrected for this effect. The uncertainty of this acceptance loss correction can introduce a systematic uncertainty (section 2.2.1).

- Because of the similarity of the K_{e2} and $K_{\mu 2}$ kinematics, the effect from acceptance distortions is drastically reduced. However, since the detector acceptance is obtained by a simulation calculation, the imperfect reproducibility of the experimental spectra by the Monte Carlo simulation can introduce a systematic uncertainty (section 2.2.2).

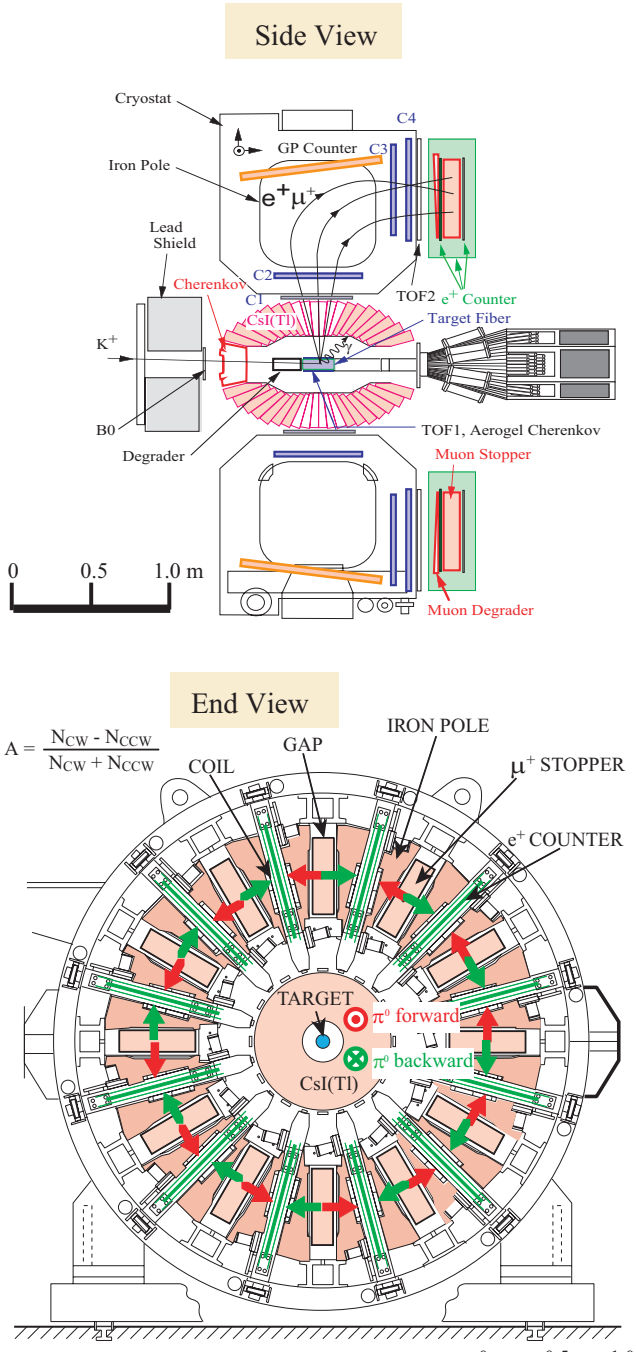

Figure 1: Cross sectional end- and side- views of the setup for the R_K experiment and the heavy neutrino search. The momentum vectors of charged particles and photons are determined by the toroidal spectrometer and the CsI(Tl) calorimeter, respectively.

- An efficiency difference of the GEM and MWPCs between the e^+ and μ^+ can introduce a systematic uncertainty in the R_K measurement. Note dead channels in the tracking system do not contribute to a systematic uncertainty because it would be a common effect for K_{e2} and $K_{\mu 2}$ decays (section 2.2.3).

- The structure dependent (SD) component of the radiative $K_{e2\gamma}$ decay is a background, and we have to subtract it from the selected K_{l2} events. Any misunderstandings of the SD component of the $K_{e2\gamma}$ decay can introduce a systematic uncertainty (section 2.2.4).

(2) PID performance

- The e^+-μ^+ mis-identification can introduce a systematic uncertainty. The mis-identified μ^+ as an e^+ is very dangerous because the $K_{\mu 2}$ decay, which is 10^5 more intense than K_{e2}, can be mis-identified as a K_{e2} decay through the tail part of the PID spectra (section 2.3.1).

- $K_{\mu 2}$ decays with decay-in-flight μ^+ inside the aerogel Cherenkov (AC) detector can be accepted as K_{e2} decays. Misunderstanding of this background fraction can introduce a systematic uncertainty (section 2.3.2).

- $K_{\mu 2\gamma}$ decays with $e^\pm$ generation through electro-magnetic interaction of a radiated photon with the target material can be mis-identified as a K_{e2} decay event. Although they are basically rejected by the TOF analysis, misunderstanding of the background fraction can introduce a systematic uncertainty (section 2.3.3).

(3) Background contaminations

- Event losses due to accidental beam backgrounds. Beam particles hitting the calorimeter will be recognized as γs from K^+ decay and these events will be rejected by the analysis. (section 2.4.1)

- π^+ particles in the K1.1BR beam can generate signals in the aerogel Cherenkov counter. If these π^+s accidentally coincide with the secondary particles from the K^+ decays, these could be identified as e^+. (section 2.4.2)

- K^+ can be converted into K^0 through a charge exchange reaction during the K^+ stopping process. The K_S component can decay around the target system and has to be identified. (section 2.4.3)

In the following sections, the details of the error evaluation of each item are described.

2.2 Systematic uncertainty due to misunderstanding of the detector acceptances

2.2.1 Uncertainty of high energy external bremsstrahlung emission

Events with e^+ momentum lower than the K_{e3} endpoint due to high energy bremsstrahlung generation cannot be used in the analysis, representing an acceptance loss. This fraction was estimated to be 3.8%, and the uncertainty of this acceptance loss correction clearly introduces a systematic uncertainty. In particular, since the probability of the bremsstrahlung emission is proportional to the flight path in the target, as shown in Fig. 2, the systematic uncertainty of the R_K measurement arises from the imperfect reproducibility of the flight path distribution in the Monte Carlo simulation. In order to reduce this effect, the K^+ stopping profile should be experimentally obtained and used as input into the simulation calculation. The K^+ profile can be measured from the particle hit positions in C1 and C2 by connecting them with a straight line without using the magnetic spectrometer.

The uncertainty will be estimated by artificially changing the K^+ decay position, taking into account the spatial resolution of the K^+ decay vertex, and the acceptance change can be adopted as this systematic uncertainty. The current design of the fiber cross section is 3×3 (mm^2), and according to the simulation calculation, the K^+ vertex resolution can be expected as $\sigma_x = \sigma_y = 1.0$ mm. The associated flight path resolution is estimated to be $\sigma_{FL} = 1.4$ mm. Smearing the flight path assuming a Gaussian fluctuation with $\sigma_{FL} = 1.4$ mm, the acceptance change is determined to be

$$\Delta\Omega/\Omega = \Delta R_K/R_K = 0.02\%, \tag{3}$$

which is interpreted as systematic uncertainty. On the other hand, effects from the stopping distribution deformation in the z(beam) direction do not change the flight path distribution in the target and this systematic uncertainty is much smaller than the above effect.

2.2.2 Imperfect reproducibility of the experimental spectra by the simulation

An imperfect reproducibility of the experimental spectra by the Monte Carlo simulation can introduce a systematic uncertainty because the detector acceptance is obtained from the simulation calculation. Although the uncertainties associated with the measurement can be reduced by forming the ratio of K_{e2} and $K_{\mu 2}$ events, imperfect reproducibility of the experimental conditions by the simulation can contribute to the systematic uncertainties. In order to confirm the correct understanding of the experimental conditions, it is very important for the R_K analysis to compare the various K_{e2} and $K_{\mu 2}$ experimental spectra with the simulation. We will judge correctness of our simulation code from the good reproducibility of the experimental spectra.

In addition to the K_{e2} and $K_{\mu 2}$ decays, some of the major decay channels such as $K^+ \to \pi^0 e^+ \nu$ (K_{e3}), $K^+ \to \pi^0 \mu^+ \nu$ ($K_{\mu 3}$), and $K^+ \to \pi^+ \pi^0$ ($K_{\pi 2}$) can be used for

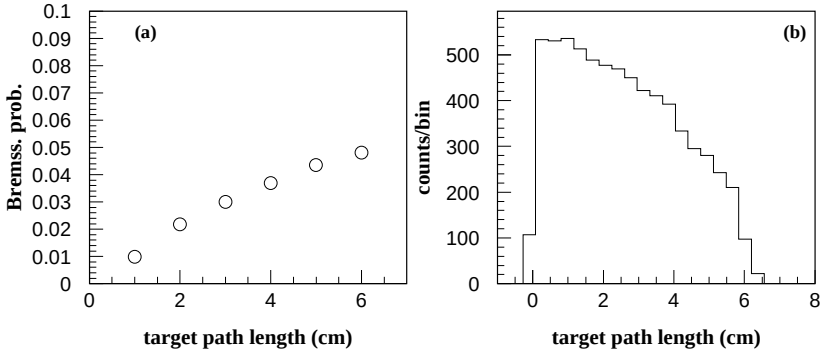

Figure 2: (a) bremsstrahlung emission probability as a function of flight path, (b) flight path distribution of the K_{e2} events in the target.

checking the experimental reproducibility. These studies have already been performed using the previous E246 and E470 experimental data, as shown in Figs. 3 and 4 [3, 4, 5, 6, 7]. The opening angles between the charged particle and the π^0 are shown in Fig. 3(a) for $K_{\mu 3}$, Fig. 3(c) for K_{e3}, and Fig. 4(b) for $K_{\pi 2}$. The charged particle momenta without the energy loss correction in the target are shown in Fig. 3(b) for $K_{\mu 3}$, Fig. 3(d) for K_{e3}, and Fig. 4(a) for $K_{\pi 2}$. The solid and dotted lines are the experimental spectra and the Monte Carlo simulation, respectively. The experimental reproducibility is very good and the reduced χ^2 values were obtained to be (a) 1.12, (b) 0.94, (c) 1.10, and (d) 1.07 for Fig. 3 and (a) 1.07 and (b) 0.96 for Fig. 4. So far, we have not found any systematic displacements of the experimental spectra from the simulation in the E246/470 experiment, and the experimental errors ($\sim 1\%$ level) such as the $\Gamma(K^+ \to \pi^0\mu^+\nu)/\Gamma(K^+ \to \pi^0 e^+\nu)$ measurement have been dominated by the statistical ones. The number of the accepted events in the P36 experiment will be expected to be 100 times higher than that in the E246/470 experiment, and one can determine accuracy of fit parameters to be 0.1% level and should be able to evaluate the reproducibility of the acceptances at the level of 0.1%. It might be necessary to tune some parameters in the simulation code in this study. We will continue these studies in the P36 experiment using the K_{e3}, $K_{\mu 3}$, and $K_{\pi 2}$ decays as well as the K_{e2} and $K_{\mu 2}$ decays.

Moreover, the branching ratios of the $K_{\pi 2}$, K_{e3}, and $K_{\mu 3}$ decays have been reported by PDG as,

$$Br(K_{\pi 2})/Br(K_{\mu 2}) = 0.3252 \pm 0.0016(0.5\%) \quad (4)$$

$$Br(K_{\mu 3})/Br(K_{e3}) = 0.6608 \pm 0.0030(0.5\%) \quad (5)$$

and these values can be used for checking the correctness of the acceptance calculation, although it is limited to the precision of 0.5%. Also, we can perform the analysis by

separating the events into several bins differentially. The R_K values can be determined in each bin and they should be consistent within errors if the analysis is successful. Any fluctuations of the R_K values which is higher than the statistical errors can be treated as the systematic uncertainty.

In summary, systematic uncertainties may arise from inconsistency of the experimental and simulation spectra. However, we will aim at achieving a systematic uncertainty better than

$$\Delta R_K / R_K < 0.1\% \tag{6}$$

by carefully analyzing the following items:

- The reproducibility of various K_{e2} and $K_{\mu 2}$ spectra by the Monte Carlo simulation.
- The reproducibility of K_{e3}, $K_{\mu 3}$, $K_{\pi 2}$ spectra by the Monte Carlo simulation.
- Comparison of the measured $Br(K_{\pi 2})/Br(K_{\mu 2})$ and $Br(K_{\mu 3})/Br(K_{e3})$ values with the results reported by PDG.
- Analysis separating the events into several bins differentially to check the consistency of the results obtained in each bin.

We will take care of these effects at the analysis stage and the systematic uncertainties will be reduced.

2.2.3 Effect from efficiency difference between e^+s and μ^+s for particle trackers

An efficiency difference of the GEMs and MWPCs between e^+ and μ^+ can introduce a systematic uncertainty in the R_K measurement. In order to remove this systematic effect, their efficiencies will be directly determined using the experimental data. In the R_K measurement, four tracking elements are used; however the trigger condition does not include their signals. The efficiency can be determined by comparing signals from a particular element with the tracks reconstructed by the others. By changing the combination of the elements, as shown in Table 1, we can determine the efficiency of all the tracking elements for each particle species e^+ and μ^+.

As mentioned in section 7.2.3 of the original P36 proposal, we can easily accumulate 10^4 events due to K_{e3} and $K_{\mu 3}$ by changing the magnetic field of the spectrometer to $B = 0.9$ T. The particle identification can be done by using the TOF and AC measurements[1], and therefore the μ^+/e^+ separation should be very reliable.

The tracking efficiency (ϵ_t) can be described as,

$$\epsilon_t = \epsilon_1 \cdot \epsilon_2 \cdot \epsilon_3 \cdot \epsilon_4, \tag{7}$$

[1]We can use the PGC counter in this measurement, if necessary. See section 2.3.1

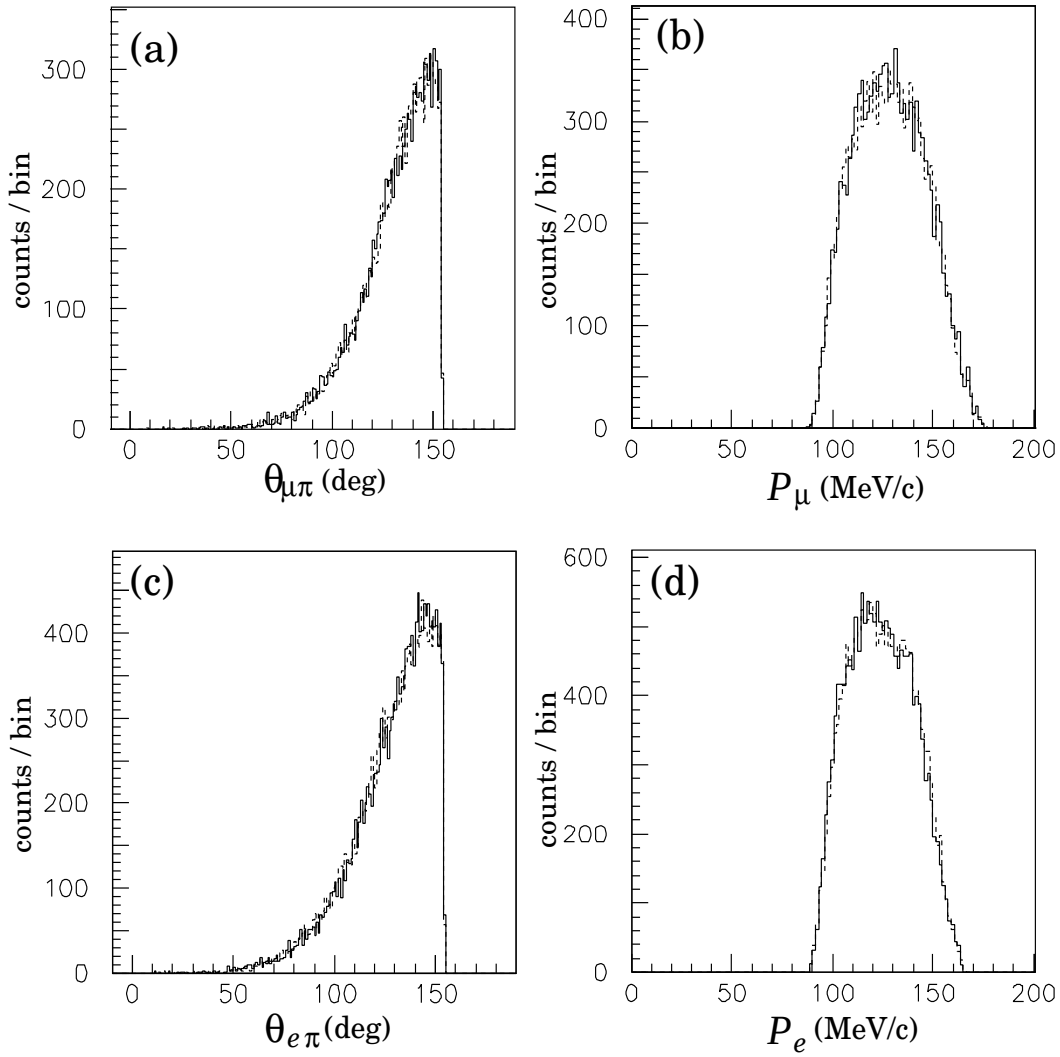

Figure 3: K_{e3} and $K_{\mu 3}$ spectra in the E246 experiment [4]: (a)(c) are the opening angle distributions between the charged particle and the π^0, (b)(d) are the charged particle momenta without any energy loss correction in the target. The solid and dotted lines are the experimental data and the Monte Carlos simulation, respectively.

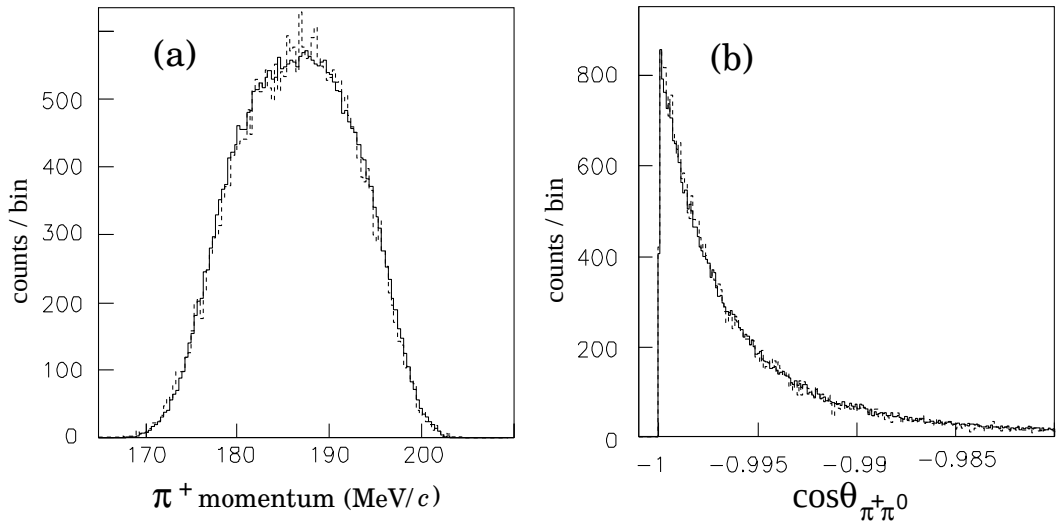

Figure 4: $K_{\pi 2}$ spectra measured in the E246 experiment [3]. (a) is the π^+ momentum without any energy loss correction in the target. (b) is the opening angle between the π^+ and the π^0. The solid and dotted lines are the experimental data and the Monte Carlos simulation, respectively.

where ϵ_i is the efficiency of Ci chamber. The statistical uncertainty of the particle tracking efficiency is

$$(\frac{\Delta\epsilon_t}{\epsilon_t})^2 = (\frac{\Delta\epsilon_1}{\epsilon_1})^2 + (\frac{\Delta\epsilon_2}{\epsilon_2})^2 + (\frac{\Delta\epsilon_3}{\epsilon_3})^2 + (\frac{\Delta\epsilon_4}{\epsilon_4})^2, \quad (8)$$

$$\frac{\Delta\epsilon_t}{\epsilon_t} < 2 \times \frac{\Delta\epsilon_g}{\epsilon_g} \quad (9)$$

where ϵ_g is the worst efficiency among the four. The uncertainty of the tracking efficiency is at most about a factor of 2 worse than that of each tracker efficiency. The number of the K_{e3} events is estimated by assuming the following conditions

- K^+ beam intensity is I_K =220 kHz,
- K^+ stopping efficiency is f =0.2, and
- Detector acceptance for K_{e3} is $\Omega(K_{e3})$ =0.01,

as,

$$N(K_{e3}) = I_K \times f \times Br(K_{e3}) \times \Omega(K_{e3}) = 7.9 \times 10^4 (/\text{hour}). \quad (10)$$

To achieve $\Delta\epsilon_t/\epsilon_t \leq 0.1\%$, $\Delta\epsilon_g/\epsilon_g$ should be obtained with an accuracy of 0.05%, which corresponds to $N(K_{e3}) = 4 \times 10^4$ assuming a chamber efficiency is ϵ_g =99%. Therefore, we can easily accumulate sufficient K_{e3} events within a few hours for

Table 1: Summary of the performance check for the tracking elements. The efficiency can be determined by comparing signals from a particular element with the tracks reconstructed by the others.

Element for check	Tracking elements	PID
C1	C2, C3, C4	TOF⊗AC
C2	C1, C3, C4	TOF⊗AC
C3	C1, C2, C4	TOF⊗AC
C4	C1, C2, C3	TOF⊗AC

checking the efficiency of the particle trackers. In other words, assuming ϵ_g =99% and one hour data collection with B=0.9 T, we can determine the systematic uncertainty due to tracking efficiency up to a level of

$$\Delta R_K/R_K = \Delta\epsilon_t/\epsilon_t = 0.035\%, \tag{11}$$

by following Eqs. (48) and (49) from the P36 proposal. For the determination of the muon efficiency, the $K_{\mu 2}$ events are used and the statistical uncertainty $\Delta\epsilon_t/\epsilon_t$ is even smaller.

2.2.4 Misunderstanding of the SD component in D0 sample

In the R_K measurement, the structure dependent (SD) component of the radiative $K_{e2\gamma}$ decay is a background, and we have to subtract it from the selected events in the D0 sample (no γ events) [2]. The D0 sample contains $K_{e2\gamma}^{SD}$ events with a photon escaping from the holes, and therefore the uncertainty of this background estimation introduces a systematic uncertainty. On the other hand, the SD component is also recorded in the alternative D1 sample (1 γ events) with significant statistics. We can analyze these data in order to understand the nature of the radiative $K_{e2\gamma}$ process. The correct understanding of the SD spectra in the D1 data, in terms of the form factors [8, 9] in the SD process from the simulation calculation, makes the uncertainty of the $K_{e2\gamma}^{SD}$ backgrounds in the D0 data statistically small enough. However, we would like to make a conservative estimation of the uncertainty from this analysis using the $K_{e2\gamma}^{SD}$ results reported by the KLOE group [2].

Here, we can estimate the systematic uncertainty using the central values of the $K_{e2\gamma}^{SD}$ form factor reported by the KLOE group as, $V + A = 0.125 \pm 0.007$ and $\lambda = 0.38 \pm 0.21$ [2]. The error sizes should be scaled taking into account the number of the accepted $K_{e2\gamma}^{SD}$ events in KLOE (1378) and P36 (40000). Therefore, in this uncertainty estimation,

$$V + A = 0.125 \pm 0.001, \tag{12}$$

$$\lambda = 0.38 \pm 0.03. \tag{13}$$

[2]The definition of D0 and D1 are explained in section 4.5 in the P36 proposal.

are adopted. By changing the form factor within the errors, the number of the accepted radiative SD events is determined to be

$$\Delta N(SD)/N(SD) = 0.075\%. \tag{14}$$

The SD background fraction in the D0 sample is estimated to be 7.2% and the corresponding R_K change is

$$\Delta R_K/R_K = 0.072 \times 0.075\% = 0.005\% \tag{15}$$

Also, we have to take into account the statistical uncertainty of this background subtraction. The numbers of the $K^{SD}_{e2\gamma}$ events accepted as D0 and D1 are $N(SD, 0\gamma) = 18 \times 10^3$ and $N(SD, 1\gamma) = 40 \times 10^3$, respectively. The probability to be assigned as D0 is

$$k = \frac{N(SD, 0\gamma)}{N(SD, 1\gamma)} = \frac{18k}{40k} = 0.45. \tag{16}$$

The statistical uncertainty of $N(SD, 0\gamma)$ is obtained as,

$$\frac{\Delta N(SD, 0\gamma)}{N(SD, 0\gamma)} = \frac{k\sqrt{N(SD, 1\gamma)}}{N(SD, 0\gamma)} = 0.005. \tag{17}$$

The uncertainty of the SD background subtraction is obtained by repeating the same calculation mentioned above as,

$$\Delta R_K/R_K = 0.072 \times 0.5\% = 0.036\%, \tag{18}$$

which is a factor of 7 larger than the effect from the form factor ambiguity, and thus treated as the systematic uncertainty due to the K^{SD}_{e2} background.

2.2.5 Theoretical ambiguity of radiative correction

The radiative correction is a higher order QED effect through the radiative $K_{e2\gamma}$ process which is theoretically calculable. We can check the theoretical calculation [10] by comparing with the experimental results recorded in the D1 sample (1 γ events). The uncertainty can be estimated from the experimental reproducibility by the Monte Carlo simulation. Therefore, it is mandatory to include the effect of radiated photons in the Monte Carlo (MC) simulations. The main problem in simulating radiative decays is the presence of infrared divergences: the total decay width for single photon emission, computed at any fixed order in α, is infinite. By extending the soft-photon approximation of [11] to the whole energy range, the problem of infinite probabilities in radiative processes is solved [10]. The systematic uncertainty can be further reduced by using the full $O(p^4)$ calculations for the amplitudes. It should be noted that the contribution from this effect was estimated to be negligible in the latest results

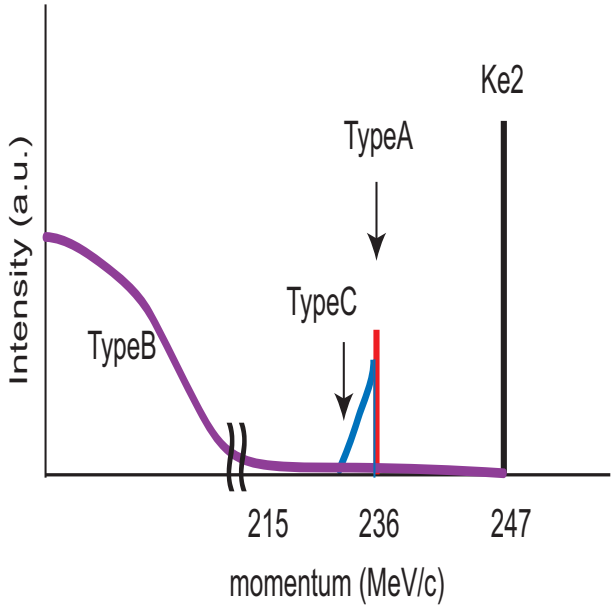

Figure 5: Schematic momentum distribution of various backgrounds after requiring an e^+ by the TOF and AC measurement. Type A: $K_{\mu 2}$ events due to mis-identification by TOF and Cherenkov (Sec. 2.3.1). Type B: $K_{\mu 2}$ events with an in-flight μ^+ decay before reaching the AC counter (Sec. 2.3.2). Type C: $K_{\mu 2\gamma}$ events with the $e^\pm$ creation by a radiated photon (Sec. 2.3.3).

reported by the NA62 group [1]. Here, we estimate the small systematic uncertainty as

$$\Delta R_K / R_K \ll 0.1\%, \tag{19}$$

which should be much smaller than the uncertainty from the effect of the imperfect reproducibility of the experimental condition in the simulation described in section 2.2.2.

2.3 PID performance

In general, any mis-identification of an e^+ as a μ^+ is harmless, while mis-identification of a μ^+ as an e^+ is rather dangerous because the $K_{\mu 2}$ decay is 10^5 more intense than the K_{e2} decay. The $K_{\mu 2}$ decay can be mis-identified as K_{e2} through (I) the tails of the TOF and AC spectra (Type-A, section 2.3.1), (II) in-flight μ^+ decay inside the AC counter (Type-B, section 2.3.2), (III) $e^\pm$ creation from a radiated photon in $K^+ \to \mu^+\nu\gamma$ (Type-C, section 2.3.3). The schematic charged particle momentum distributions of these 3 processes are shown in Fig. 5.

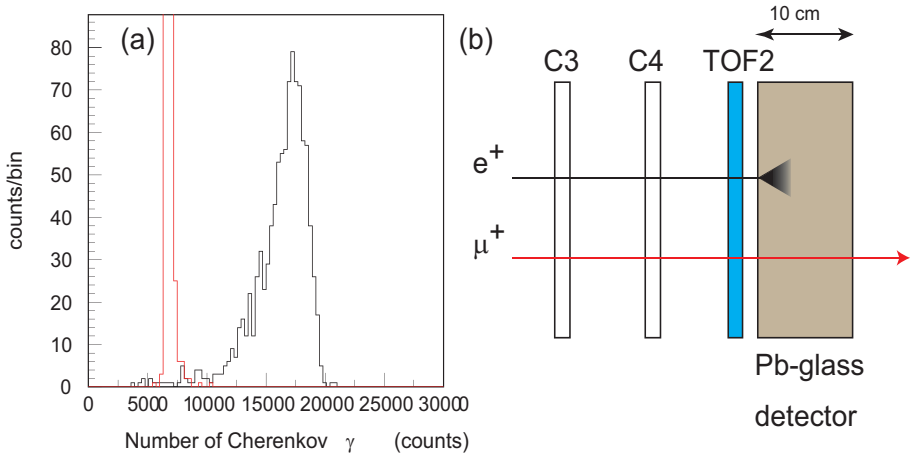

Figure 6: (a) Cherenkov photon yields generated by e^+ and μ^+ hits in the 10 cm Pb-glass material by a Monte Carlo simulation and (b) schematic view of the new PGC detector system. A Pb-glass Cherenkov material of 10 cm in thickness will be placed behind the TOF2 counter. The black and red histograms in (a) correspond to e^+ and μ^+ signals, respectively.

2.3.1 Effects from particle mis-identification by TOF and AC

Before starting the discussion for this uncertainty estimation, we would like to mention an additional Pb-glass Cherenkov detector (PGC) with 10 cm in thickness, which has not been described in the original P36 proposal. The PGC will be placed just behind TOF2 in all magnet gaps, as shown in Fig. 6(b). This detector plays a supplementary role in the particle identification for the TOF and AC efficiency determinations. The properties of the PGC system can be summarized: reflective index $n = 1.67$, density $\rho = 4.97$ g/cm^3, Pb fraction 57%, and radiation length $X_0 = 2.33$ cm. The number of Cherenkov photons generated in the detector have been obtained by a Monte Carlo simulation based on a GEANT4 code, as shown in Fig. 6(a). Here, the light collection efficiency to a photon detector and the efficiency of the photon detector is not taken into account. The black and red histograms correspond to e^+ and μ^+ signals, respectively. Putting a threshold level corresponding to 10000 photons, the detection efficiencies for μ^+ and e^+ are expected to be 100% and 99.8%, respectively. The probability to mis-identify e^+ as μ^+ is 0.2%. By combining the new Pb-glass counter with the AC counter and/or TOF system, we can identify the charged particles with high precision.

It is clear that particle mis-identification introduces an additional uncertainty for the R_K determination. In order to check the performance of the particle identification by the TOF and AC system, the mis-identification probability will be directly measured using the experimental data, which is very similar method mentioned in section 2.2.3. Here, the PGC system is available and it will help to confirm the particle identification for this calibration purpose. The probability of the e^+ inefficiency

Table 2: Summary of the performance check for the particle ID. The PGC detector plays a supplementary role in the PID probability measurements for the AC and the TOF systems. The PID probability can be determined by changing the combination of AC, TOF, and PGC.

Element for check	Tracking elements	PID
AC	C1, C2, C3, C4	TOF⊗PGC
TOF	C1, C2, C3, C4	AC⊗PGC
PGC	C1, C2, C3, C4	TOF⊗AC

and the μ^+ mis-identification by the AC counter can be measured by comparing the AC signals with the TOF and PGC information. It is to be noted that four-point tracking can be used for this study. By changing the combination of the detectors and repeating the calibration, we can check the performance of all three detectors, as shown in Table 2. The systematic uncertainty due to non-ideal performance of the particle identification is subject to the statistical uncertainty of these efficiency determinations.

Here we will use the K_{e3} and $K_{\mu 3}$ events which can be easily accumulated to a level of 10^4 events by changing the spectrometer field to B=0.9 T. Removing the TOF2, AC, and PGC signals from the trigger and adding the C4 signals into the trigger, the data will be collected. The statistical error of the efficiency determination is the same as the results obtained in section 2.2.3. Assuming 1% mis-identification probability and one hour data collection with B=0.9 T, the systematic uncertainty due to non-ideal performance of the particle identification is expected to be controlled to a level

$$\Delta R_K/R_K = 0.035\%, \tag{20}$$

following the procedure of Eq.(10) in section 2.2.3,

The $K_{\mu 2}$ background fraction can be estimated from the charged particle momentum spectrum by requiring the e^+ conditions by the TOF and AC information. The $K_{\mu 2}$ fraction can be determined by fitting the momentum distribution around the $K_{\mu 2}$ peak with a reasonable function. Note the background $K_{\mu 2}$ events have a momentum of 236 MeV/c, as shown in Fig. 5 (Type-A).

2.3.2 In-flight μ^+ decay

Events with in-flight μ^+ decay ($\mu^+ \to e^+\nu\bar{\nu}$) from $K_{\mu 2}$ before reaching the aerogel Cherenkov counter might be accepted as K_{e2}, although the AC will be placed as close as possible to the K^+ stopper. In particular, the endpoint of the e^+ momentum from $K_{\mu 2}$ decay is the same as the e^+ momentum from K_{e2} decay, as shown in Fig. 5 (Type-B). Since the endpoint events correspond to the μ^+ forward boosted case, it is difficult to remove them by a momentum analysis only.

Taking the current design value for the distance between the K^+ decay position and the inner radius of AC to be 6 cm, the μ^+ decay probability (f) is calculated to be

$$l = \beta\gamma c\tau = 1494\text{m} \quad (21)$$
$$f = 1 - \exp(0.06/1494) = 4.0 \times 10^{-5}. \quad (22)$$

However, taking into account the K_{e2} and $K_{\mu 2}$ branching ratios, the number of the $K_{\mu 2}$ background events per K_{e2} events is obtained to be

$$f \times Br(K_{\mu 2})/Br(K_{e2}) = 1.6. \quad (23)$$

This value is not small, however, the e^+ momentum is much smaller than the momentum region of interest, as shown in Fig. 7(a),(b). The red, blue, and pink lines in Fig. 7(b) correspond to the K_{e3} endpoint, and the $K_{\mu 2}$ and K_{e2} momenta, respectively. The opening angle between the e^+ and the μ^+ ($\theta_{e\mu}$) and the scatter plot of the e^+ momentum and $\theta_{e\mu}$ are also shown in Fig. 7(c) and (d), respectively. The surviving fraction of these events after requiring that the e^+ momentum is higher than 228 MeV/c is obtained to be 1.2×10^{-3}. Taking into account this rejection power, the background fraction is estimated to be

$$f \times Br(K_{\mu 2})/Br(K_{e2}) \times 1.2 \times 10^{-3} = 0.19\% \quad (24)$$

which should be subtracted from the K_{e2} sample. Since this background fraction is calculable from the muon decay kinematics, the uncertainty is very small. Here assuming this uncertainty to be better than 5%, the error size is expected $< 0.19\times$ 5% = 0.0095%.

On the other hand, the in-flight μ^+ decay inside the AC can contribute to the systematic uncertainty because the e^+ efficiency strongly depends on the AC performance and the μ^+ decay position. Taking into account the AC thickness of 2 cm, this fraction is obtained to be 0.05% of the number of the total K_{e2} events. In principle, we can estimate the AC efficiency for these events relying on the simulation code. Here assuming a modest value of this uncertainty to be 50% (outer half of the detector is sensitive), the systematic uncertainty due to in-flight μ^+ decay from the $K_{\mu 2}$ is adopted to be

$$\Delta R_K/R_K = 0.05\% \times 0.5 = 0.025\%, \quad (25)$$

which can be improved by understanding the details of the AC performance from a comparison of the test experimental data (see section 5) with the simulation.

2.3.3 $e^\pm$ creation from a radiated photon in $K^+ \to \mu^+\nu\gamma$ decay

$K_{\mu 2\gamma}$ events with $e^\pm$ generation through interactions (photoelectric effect, Compton scattering, $e^\pm$ pair production) of the radiated photons with electrons in the target

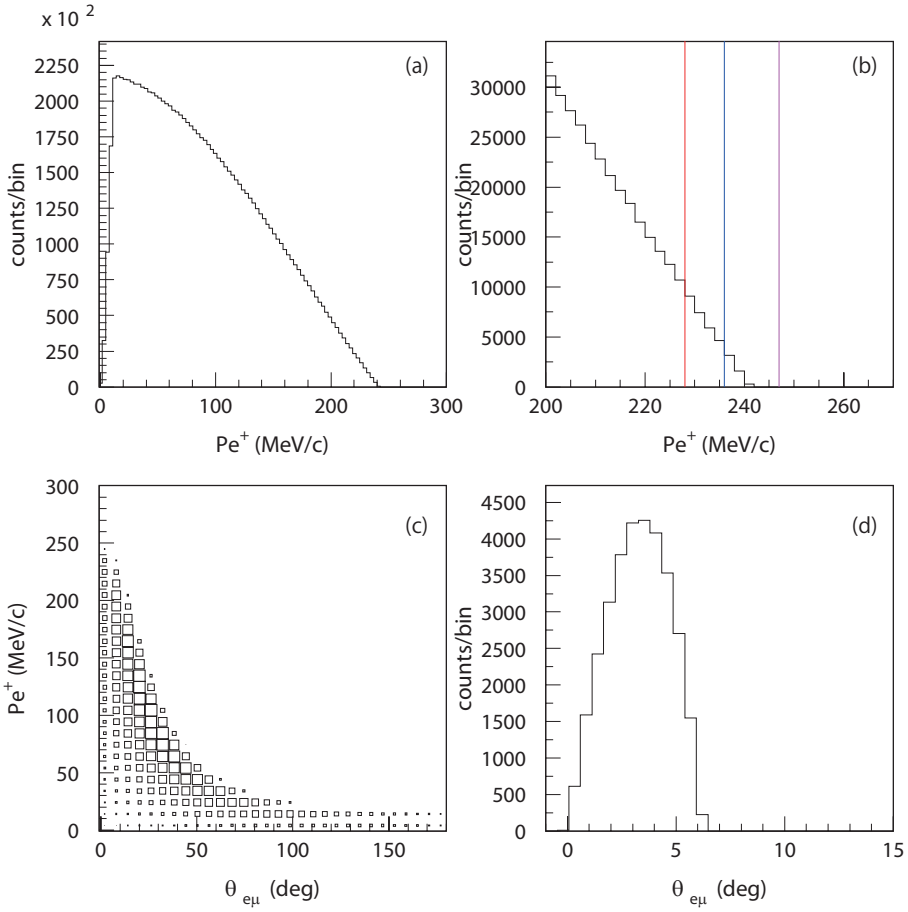

Figure 7: The e^+ spectra of in-flight $\mu^+ \to e^+\nu\bar{\nu}$ decay from the $K_{\mu 2}$ decay: (a) e^+ momentum, (b) e^+ momentum in the high momentum region, (c) scatter plot of the e^+ momentum and $\theta_{e\mu}$, (d) $\theta_{e\mu}$. The red, blue, and pink lines in (b) correspond to the K_{e3} endpoint, and the $K_{\mu 2}$, and K_{e2} momenta, respectively. The surviving fraction of these events after requiring that the e^+ momentum is higher than 228 MeV/c is obtained to be 1.2×10^{-3}.

materials would be mis-identified as K_{e2}. For example, $e^{\pm}$ generated in the TOF1 counter through which the μ^+ passes will make a signal in the aerogel Cherenkov counter, and the μ^+ which coincides with the generated $e^{\pm}$ turns out to be identified as an e^+. Fig. 8(a) shows the $e^{\pm}$ arrival probability ($\rho(E_\gamma)$) at the AC counter as a function of the original photon energy. Fig. 8(b) is the photon energy distribution of the $K_{\mu 2\gamma}$ decay, where the vertical axis is normalized so that the gross integration over the entire region is 1. However, since the charged particle mass obtained from the TOF measurement is the muon rest mass, we can remove these events by TOF analysis. The number of these background events, $N(K^{BG}_{\mu 2\gamma})$, can be expressed as,

$$N(K^{BG}_{\mu 2\gamma}) \propto \int \Omega(K_{\mu 2\gamma}) \cdot Br(K_{\mu 2\gamma}, E_\gamma > 1.6\mathrm{MeV}) \cdot \rho(E_\gamma) \cdot \epsilon_{TOF} \cdot dE_\gamma, \tag{26}$$

where $\Omega(K_{\mu 2\gamma})$ is the detector acceptance and ϵ_{TOF} is the suppression factor by the TOF analysis. $Br(K_{\mu 2\gamma}, E_\gamma > 1.6\mathrm{MeV})$ denotes the partial branching ratio with photon energy higher than 1.6 MeV. Also, the number of the accepted K_{e2} events, $N(K_{e2})$, is described using a similar form as,

$$N(K_{e2}) \propto \Omega(K_{e2}) \cdot Br(K_{e2}) \cdot 1 \cdot 1. \tag{27}$$

The $K^{BG}_{\mu 2\gamma}$ fraction can be obtained as $N(K^{BG}_{\mu 2\gamma})/N(K_{e2}) = 2.2 \times \epsilon_{TOF}$. As discussed in section 2.3.1, the ϵ_{TOF} value can be directly measured using the experimental data. Here assuming $\epsilon_{TOF} = (1 \pm 0.1) \times 10^{-3}$, the uncertainty is estimated to be

$$\Delta R_K / R_K = N(K^{BG}_{\mu 2\gamma})/N(K_{e2}) = 0.02\%. \tag{28}$$

It is to be noted that the charged particle momentum of these events is different from that of the K_{e2} decay, as shown in Fig. 5 (Type-C).

2.4 Systematic uncertainties due to background contaminations

Systematic uncertainty can arise from beam backgrounds. In general, effects from accidental beam backgrounds are common for the K_{e2} and $K_{\mu 2}$ decays, and we can reduce them by calculating the ratio $N(K_{e2})/N(K_{\mu 2})$. By requiring a timing cut on the K^+ transit time (Δ_t) in the K^+ stopper obtained from time difference between the K^+ Cherenkov counter and the TOF1 counter, we can remove events corresponding to in-flight K^+ decays. Also, K^0 events generated through a charge exchange reaction from K^+ during the stopping process can be rejected.

2.4.1 Mis-identification of beam particles hitting to the CsI(Tl) calorimeter as photons from the target

Beam particles hitting the calorimeter can be mis-identified to be γs from K^+ decay. These events should be recorded in the D0 sample (no γ events); however due to

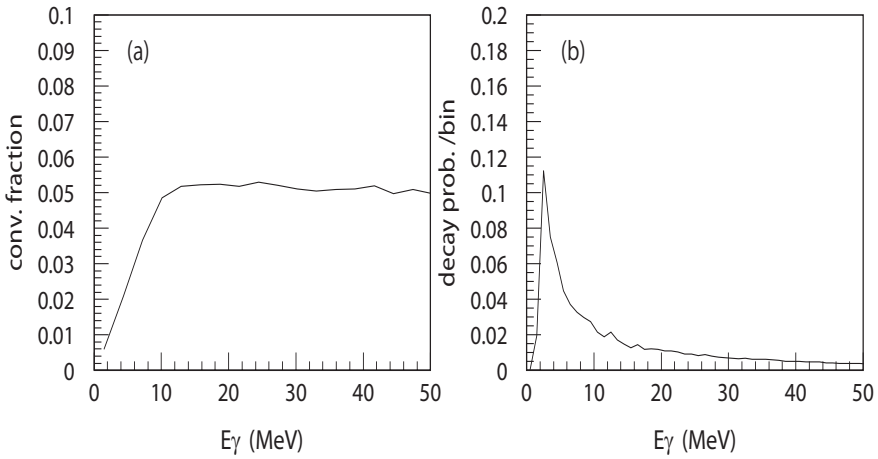

Figure 8: (a) is the $e^{\pm}$ arrival probability at the AC counter as a function of the original photon energy. (b) is the photon energy distribution of the $K_{\mu 2\gamma}$ decay, where the vertical axis is normalized such that the gross integration over the entire region is 1. Fine structure in the spectra is due to the statistical fluctuation.

the existence of these backgrounds they would be identified in the D1 sample (1 γ events), changing the numbers of the accepted events. However, these backgrounds are accidental events and they are common for K_{e2} and $K_{\mu 2}$. Therefore, by forming the ratio of the accepted K_{e2} to $K_{\mu 2}$ numbers, this effect is basically cancelled out. The statistical uncertainty of this event reduction is

$$\Delta/N(K_{l2}) = \sqrt{\epsilon(1-\epsilon)}/\sqrt{N(K_{l2})}, \tag{29}$$

where ϵ is the event loss probability due to this background contamination. We will make every effort to reduce this probability to less than 5% in the measurement. In that case, the uncertainty is estimated to be

$$\Delta R_K/R_K = 0.2\% \times 0.22 = 0.04\%. \tag{30}$$

2.4.2 Mis-identification of beam π^+ as e^+ by the aerogel Cherenkov counter

π^+ particles in the K1.1BR beam can generate signals in the aerogel Cherenkov counter. If these π^+s accidentally coincide with the secondary particles from the K^+ decay, they will be identified as e^+s. These backgrounds might be a problem taking into account the $\mathrm{Br}(K_{e2})/\mathrm{Br}(K_{\mu 2}) \sim 1.6 \times 10^{-5}$. However, these events can be basically rejected by requiring one cluster in B0, where B0 is a GEM detector located at the beam collimator of the K1.1BR beamline to record all particles during the K^+ decay period. Also, they will be removed by the TOF analysis because the mass obtained from the TOF measurement is the muon rest mass. The number of these backgrounds (N^{π}_{acci}) can be written as,

$$N^{\pi}_{acci} = N(K_{\mu 2}) \cdot \tau_{acci} \cdot n(\pi) \cdot \bar{\epsilon}_{veto} \cdot \bar{\epsilon}_{TOF}, \tag{31}$$

where τ_{acci}, $n(\pi)$, $\bar{\epsilon}_{veto}$, and $\bar{\epsilon}_{TOF}$ are the π^+ accidental coincidence probability determined from the time resolution of the AC counter, the π^+ counting rate at AC, the veto inefficiency of B0, and probability of the TOF mis-identification, respectively. Assuming τ_{acci}=1ns/1s=10^{-9}, $n(\pi) = 220 \times 10^3 \times 0.1 \times 1/6$ (Hz), $\bar{\epsilon}_{veto} = 10^{-2}$, and $\bar{\epsilon}_{TOF} = 10^{-3}$, N^{π}_{acci} is obtained to be

$$N^{\pi}_{acci} = N(K_{\mu 2}) \cdot 10^{-9} \cdot (220 \times 10^3 \times 0.1 \times 1/6) \cdot 10^{-2} \cdot 10^{-3} \quad (32)$$

$$= N(K_{\mu 2}) \times 0.37 \times 10^{-10}. \quad (33)$$

Here we assumed 10% of the beam π^+s hit the AC counter which has a structure with six sector segmentation. The background fraction can be written as

$$\frac{N^{\pi}_{acci}}{N(K_{e2})} = \frac{N(K_{\mu 2})}{N(K_{e2})} \times 0.37 \times 10^{-10} = 0.23 \times 10^{-5}. \quad (34)$$

Therefore, effect from this background is negligibly small. Event in the case of 10% duty factor, the background fraction is still less than 10^{-3} level.

2.4.3 K^+ conversion to K^0

K^+ can be converted into K^0 through a charge exchange reaction during the K^+ stopping process. The K_L component is not accepted by the TREK system due to its long lifetime (τ_{K_L} = 52 ns). We can remove the K_S component by rejecting the prompt events in the K^+ timing spectrum obtained from the incoming K^+s and outgoing secondary particles from the K^+ decay because $\tau_{K_S} = 90$ ps. Also, we can remove effects from in-flight K^+ decays by the same method. From the E246/470 experimental results, the peak width of the prompt events was obtained to be 0.5 ns in σ. Requiring the condition to be Δ_t >2 ns, the background fraction can be reduced to a level of 0.003% of the total K_{e2} and $K_{\mu 2}$, and therefore, the uncertainty can be reduced to

$$\Delta R_K/R_K = 0.003\%. \quad (35)$$

However, this prompt cut removes also genuine K_{e2} and $K_{\mu 2}$ events. Careful tuning of the cut point will be necessary in the analysis.

2.5 Summary of error estimation

In this report, we have considered the systematic uncertainties by separating them into 3 categories: systematic uncertainty due to (1) misunderstanding of the detector acceptances, (2) PID performance, and (3) background contaminations. The uncertainties from each item are summarized in Table 3. The total systematic uncertainty is obtained to be $\Delta R_K/R_K = 0.13\%$ by adding all items in quadrature, because all the items investigated are independent of each other. We can evaluate the P36 experimental strategy and prominent characteristics by considering the source of each uncertainty as follows.

- The most serious contribution is due to imperfect reproducibility of the experimental conditions in the Monte Carlo simulation, although we have not found any systematic disagreements between the experimental spectra and the simulation in the previous E246/470 experiments. We will aim at achieving a systematic uncertainty better than 0.1% by checking and controlling the consistency of the various experimental spectra with the simulation.

- We can put the AC counter close to the K^+ decay position so that in-flight $K_{\mu 2}$ events can be rejected effectively. This is one of specific characteristics of a stopped K^+ beam. On the other hand, we have to take care of interactions of secondary particles with target materials such as generation of bremsstrahlung photons and γ conversion to $e^{\pm}$.

- As shown in Table 3, the uncertainty sources are also classified into (Cat.1) misunderstanding of the detector acceptance due to detector misalignment and (Cat.2) statistical error of the efficiency correction factor.

- Some of the systematic uncertainties are expected to be improved by further studies of the detector performance and the simulation code, as shown in Table 3 as 'Imp'.

- The number of the $K^{SD}_{e2\gamma}$ events in the P36 experiment will be $\sim 4 \times 10^4$ events which is about 30 times larger than in KLOE. A reliable subtraction from the accepted K_{e2} sample is possible.

- The PID performance is very important because the $K_{\mu 2}$ decay is 10^5 more intense than the K_{e2} decay. We will introduce an additional Pb-glass Cherenkov counter which plays a supplementary role of the PID measurement in the efficiency measurement.

The NA62 group has overcome various difficulties originating with an in-flight K^+ beam and achieved a systematic error of 0.3%. We plan to refer to the NA62 analysis procedure and incorporate several ideas into the P36 analysis. By taking lessons from NA62 and applying the TREK detector system with a stopped K^+ beam, we are aiming at further improvement of the systematic error to 0.1%.

3 Theoretical calculation of the muon polarization in the $K^+ \to \mu^+ N$ decay and treatment of the muon polarization in P36

In the P36 proposal, we considered the muon polarization from the $K^+ \to \mu^+ N$ decay to be 100% assuming a pure V+A contribution to the heavy neutrino production. This was not based on correct theoretical consideration, and the PAC requested us

Table 3: Summary of the systematic uncertainties. The total systematic uncertainty is obtained to be $\Delta R_K/R_K = 0.13\%$ by adding all items in quadrature. Some of the systematic uncertainties are expected to be improved by further studies (Imp), where (o) denote a remaining possibility of the uncertainty improvement and $\times$ is already an ultimate value. The error sources are also classified into (Cat.1) misunderstanding of the detector acceptance due to detector misalignment and (Cat.2) statistical error of the efficiency correction factor. The largest contribution is the effect from the experimental reproducibility by the simulation, and we will aim at achieving a systematic uncertainty better than 0.1% by checking the consistency of various experimental spectra with the simulation.

Items	$\Delta R_K/R_K$	Imp.	Cat.1	Cat.2
(1)Uncertainty of detector acceptances				
External bremsstrahlung	0.02%	$\times$	o	-
Imperfect reproducibility by simulation	$< 0.1\%$	o	o	-
Efficiency of tracking elements	0.035%	o	-	o
SD component	0.036%	$\times$	o	-
(2)PID Performance				
e^+/μ^+ mis-identification.	0.035%	o	-	o
In-flight $K_{\mu 2}$ decay	0.025%	o	o	o
$e^\pm$ creation from $K_{\mu 2\gamma}$ decay	0.02%	o	o	o
(3)Background contaminations				
Accidental beam backgrounds in CsI(Tl)	0.04%	o	-	-
Beam π^+ in AC	<0.01%	o	-	-
K^0, and in-flight K^+ beam	<0.01%	o	-	-
Total systematic uncertainty	0.13%			
Statistical error	0.2%			

to show a more complete analysis of the polarization technique in the heavy neutrino search.

First of all, we would like to emphasize that the statistical sensitivity discussed in the P36 proposal is mainly determined by the peak search in the muon momentum distribution. The statistical error cannot be improved drastically even if a simultaneous fitting to the momentum and polarization distributions will be performed. However, the muon polarization measurement is still important and the treatment of the muon polarization in the P36 experiment is explained as follows. A peak corresponding to heavy neutrinos will be searched for in the muon momentum distribution. Then, if we successfully find some indications of peaks, we will check the muon polarization in order to confirm the existence of the peak and to reduce the systematic error. We have to withdraw the statement of simultaneous fitting and resulting improvement of the statistical error as stated in the original P36 proposal.

The muon polarization can be calculated as a function of the heavy neutrino mass as follows[3]. For the massive ν case, a μ^+ carrying the helicity + appears and the right-handed component has to be taken into account. The partial decay width (X) to muon helicity $h = +1$ and $h = -1$ states can be described as

$$X|_{h=+1} = C \cdot [(M_I^2 - m_\mu^2)m_K(E_{\mu^+} + k_{\mu^+}) + m_K^2 m_\mu^2], \quad (36)$$

$$X|_{h=-1} = C \cdot [(M_I^2 - m_\mu^2)m_K(E_{\mu^+} - k_{\mu^+}) + m_K^2 m_\mu^2], \quad (37)$$

where m_K, m_μ, and M_I are kaon, muon, and neutrino masses, respectively. E_{μ^+} is the muon energy and k_{μ^+} is the muon momentum. C is the physics parameter determined by the model. The muon polarization (P_{μ^+}) can be obtained as,

$$P_{\mu^+} = \frac{X|_{h=+1} - X|_{h=-1}}{X|_{h=+1} + X|_{h=-1}}, \quad (38)$$

$$= \frac{2(M_I^2 - m_\mu^2)m_K k_{\mu^+}}{2(M_I^2 - m_\mu^2)m_K E_{\mu^+} + 2m_K^2 m_\mu^2}, \quad (39)$$

$$= \frac{(M_I^2 - m_\mu^2)m_K^2[(1 + \frac{m_\mu^2 - M_I^2}{m_K^2})^2 - \frac{4m_\mu^2}{m_K^2}]^{1/2}}{m_K^2(M_I^2 + m_\mu^2) - (M_I^2 - m_\mu^2)^2}, \quad (40)$$

which is independent of parameters in νMSM. Thus, the muon polarization has -1 in the $M_I = 0$, and the deviation from -1 gives a signal of a finite neutrino mass. The muon peak position corresponding to the neutrino mass is shown in Fig. 9(a). Also, the muon polarization is shown in Fig. 9(b) as a function of the muon momentum. The muon polarization reverses sign at the point of $M_I = m_\mu$. Fig. 10 shows the revised momentum and polarization distribution using the above polarization form; we showed those distributions using 100% for the muon polarization in the P36 proposal. However, we reconfirm that the experimental sensitivity was determined by the peak search in the momentum distribution and the estimated sensitivity of $\mathrm{Br}(K^+ \to \mu^+ N) \sim 10^{-8}$ reported in the P36 proposal is unchanged.

[3]We owe Prof. T. Asaka for these discussions, who is one of primal person for νMSM in Japan.

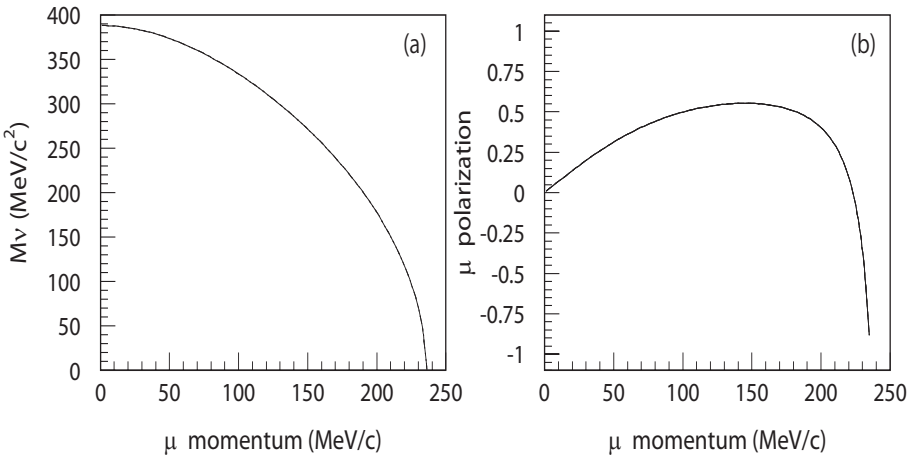

Figure 9: (a) The muon peak position corresponding to the neutrino mass and (b) the muon polarization as a function of the muon momentum. The muon polarization reverses sign at the point of $M_I = m_\mu$.

4 Results of J-PARC K1.1BR beamline commissioning

4.1 Completed K1.1BR beamline

The beamline K1.1BR, where the Superconducting Toroidal Spectrometer will be installed, and the P36 experiment will be performed, was completed in summer 2010. The TREK collaboration was responsible for the beamline commissioning and beam tuning. The optics design of this beamline was described briefly in the proposal and also in the FIFC report [12]. Further details have been presented in separate reports [13, 14] by J. Doornbos. Fig. 11 shows the layout of the completed K1.1BR channel. This beamline with a maximum beam momentum of 1.0 GeV/c can also be considered to be used for stopped beam experiments. The unique feature is the existence of an intermediate vertical focus before the electro-static separator (ESS), which enables good K/π separation in spite of a single stage ESS. Due to very tight budgetary constraints, however, the completed beam line (Fig. 11) differs from the original optics design of [14]. The different points are the following.

- The length of the ESS is not 2.5 m as in the optics design, but 2.0 m, because an old ESS from KEK-PS has been reused. This is of course disadvantageous for K/π separation.
- The bending angle of the last dipole magnet B3 is not 45 degrees as in the optics design but only 40 degrees due to the performance limit of the reused B3. This might increase the pion contamination to some extent.

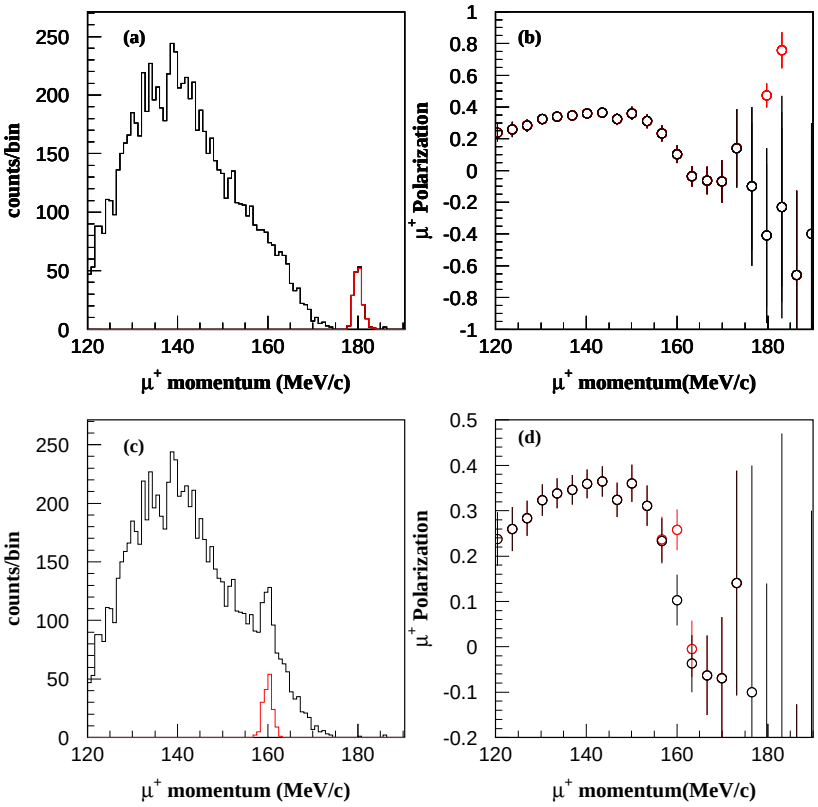

Figure 10: Distribution of (a)(c) μ^+ momentum and (b)(d) μ^+ polarization obtained by assuming $BR(K^+ \to \mu^+ N) = 2 \times 10^{-8}$ and a monoenergetic μ^+ peak (a) (b) $P_\mu = 180$ MeV/c and (c) (d)$P_\mu = 160$ MeV/c. The black (red) histograms in (a)(c) is sum of the signals and $K_{\mu 3}$ backgrounds (signal events). The red and black symbols in (b)(d) correspond to the signals and $K_{\mu 3}$ backgrounds, respectively. Here, the muon polarization is obtained by using Eq.(40), although Fig. 37 in the P36 proposal was obtained by assuming the muon polarization was 100%.

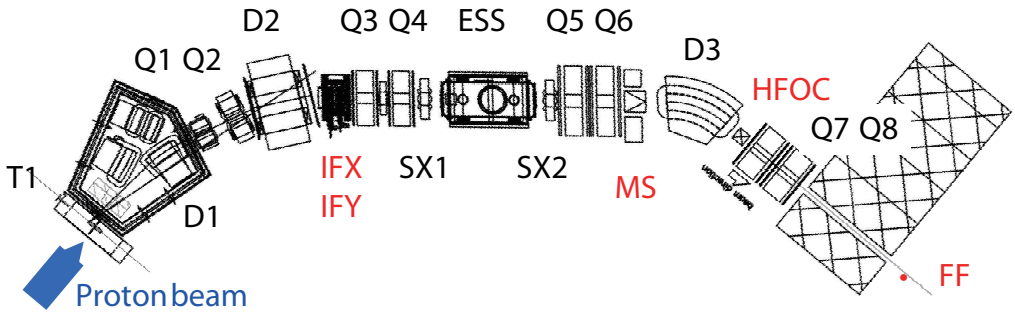

Figure 11: Layout of the completed K1.1BR beamline

It should also be mentioned that the final focus (FF) is currently 3.3 m distant from the last focusing element Q8, due to the 2.5 m thick Fe shielding, necessary for radiation safety purposes during the test beam period. This will be shortened to 0.8 m for the experiments P36 and E06. The beam tuning was carried out in October and November 2010 using 17 shifts of beam time.

4.2 K^+ intensity and K/π ratio

The kaon beam was tuned for 0.8 GeV/c beam momentum, to be used in P36 and E06, at an accelerator power of 3 kW (average) on a Pt production target. Kaons and pions were triggered independently by a Fitch-type differential Cherenkov counter, whose performance was confirmed by a TOF system. The beam survey and tuning were done with mostly narrow horizontal slit (IFX and HFOC) conditions to avoid counter performance degradation and the full intensity was deduced using a scaling factor obtained from a very narrow vertical slit (MS1 and IFY) condition. The ESS was excited to $\pm$150 kV for rough tuning and then raised to $\pm$250 kV or $\pm$300 kV for final confirmation of the K/π separation. The separation curve was measured by sweeping the E-field correction magnet (CM) current and plotting the π^+ and K^+ yields triggered by the Cherenkov detector.

Table 4 shows the obtained kaon intensity and the π/K ratio for various slit openings. The wide horizontal slits (H.S.) settings, which are relevant to the experiment, have some ambiguity due to the uncertainty of the scaling factors. The given values are lower limits, which should not be very different from the real values. For the 'standard' vertical slit openings we observed nearly 6×10^4 K^+ /spill at 3.6 kW power

Table 4: Results of K^+ beam tuning at 0.8 GeV/c at K1.1BR

Vertical slits	K^+/spill @ 3.6 kW		π/K ratio	
	Narrow H.S.	Wide H.S.	@ 250 kV	@ 300 kV
Narrow	1,253	3,629	1.4	
ΔIFY= $\pm$0.5 mm				
ΔMS= $\pm$0.75 mm				
Standard	2,541	$\geq$58,443	9.8	1.1
ΔIFY= $\pm$1.5 mm				
ΔMS= $\pm$2.0 mm				
Wide	3,493	$\geq$80,338	25.2	
ΔIFY= $\pm$2.0 mm				
ΔMS= $\pm$2.5 mm				
Widest	3,811	$\geq$87,653	26.8	6
ΔIFY= $\pm$2.5 mm				
ΔMS= $\pm$2.5 mm				

with 6 s repetition. As seen in the separation curve (Fig. 12) we achieved good separation with a π/K ratio of 1.1 on the kaon peak at the ESS operation of $\pm$300 kV. The kaon yield can be compared with that of the similar low-momentum line LESB3 [15] at BNL-AGS. Its well-established kaon beam intensity also at 0.8 GeV/c but generated with 24 GeV proton energy on a Ni production target converts to about $8 \times 10^4 K^+$/spill for the current K1.1BR condition. This indicates some more room for improvement [4].

4.3 Toward the experiment

In order to start the experiment, however, the obtained π/K ratio is not small enough. P36 as well as E06 are assuming a π/K ratio of <0.5 based on the optics calculations. The difference between 1.1 and 0.5 can be attributed to less than optimized performance of the current ESS. At this time we could investigate the expectation, when we install a 2.5 m separator, by studying decreasing behavior of pion contamination with increase of the CM current, by scaling up the deflection angle (Fig. 13). Here we assume the same electrode gap of 15 cm, and HV=$\pm$ 375 kV. We see that ratio of <0.5 should be possible. Regarding the bending angle of B3, we will be satisfied with the current condition, if a sufficient π/K ratio will be obtained by upgrading the ESS. In the present beam study we did not find any inconvenient facts.

In the beam tuning we also tried to find the optimum focusing condition at FF

[4]The accuracy of this comparison is of course limited by the ambiguity of slit openings etc. The estimate based on the Sanford-Wang formula [16] gives $6.5 \times 10^4 K^+$/spill for the current K1.1BR condition.

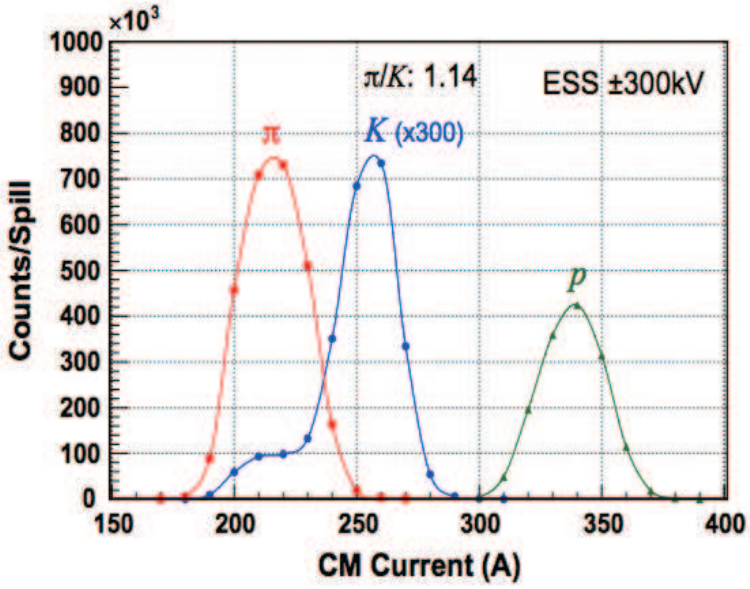

Figure 12: Mass separation curve obtained for the ESS voltage of ±300 kV at the beam momentum of 0.8 GeV/c.

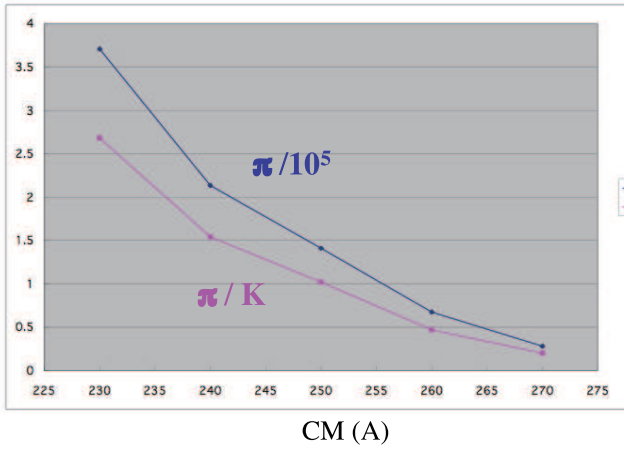

Figure 13: Expected performance of the updated ESS with the electrode length of 2.5 m, gap of 15 cm and high-voltage of ± 375 kV. The π/K ratio can be smaller than 0.5.

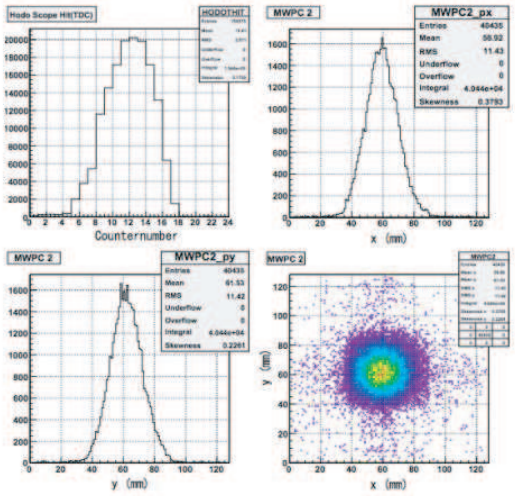

Figure 14: Kaon beam spot at the final focus (FF) for the best tuned Q7 and Q8.

(although it will be different for the nearer FF without the 2.5 m wall), by varying the last focusing elements Q7 and Q8. As is illustrated in Fig. 14 we succeeded to focus the kaon beam to a round spot with σ_x=σ_y =11 mm.

It might be too early to re-estimate the expected statistical sensitivity based on the first beam commissioning data; as mentioned above there is still a possibility to improve the beam intensity. However, it is worthwhile to have some outlook. The standard value of $6 \times 10^4 K^+$/spill @ 3.6 kW at the far FF corresponds to $9 \times 10^4 K^+$/spill at the near FF. This value converts to $7.5 \times 10^5 K^+$/spill @ 30 kW. Because we need 10^{12} K^+ this means 1.3×10^6 spills with the same time structure condition of 6 s repetition. Thus, we need roughly 10^7 s. In order to shorten the run time as much as possible toward the original plan of 50 days, The choice of 50 kW accelerator condition and more crucial settings of the slits openings (approaching 'wider' settings), compromising with the π/K ratio might become necessary.

5 Aerogel Cherenkov counter

An aerogel Cherenkov (AC) counter is a powerful tool for the e^+/μ^+ identification because positrons from the K_{e2} decays generate signals in this counter while muons from the $K_{\mu 2}$ decays does not make any signals. Hence, this counter is very important for the K_{e2} and $K_{\mu 2}$ separation in the P36 experiment. We have intensively studied the design of this counter which have been only conceptually presented in the original P36 proposal. We performed a detailed Monte Carlo study in order to maximize the e^+ detection efficiency. Then, a prototype AC counter was constructed and a

test experiment of the prototype counter using an e^+ beam was carried out. The preliminary results of data analysis is reported below.

5.1 Aerogel Cherenkov counter design

The AC counters are located between the TOF1 and the CsI(Tl) barrel, as shown in left-hand side of Fig. 15. The counter consists of 6 units of trapezoidal cross section. The length of an AC box containing the aerogel radiator along the K^+ beam axis is 220 mm to cover the whole K^+ stopping distribution. The unique feature of the unit is the separation of an aerogel radiator volume and an air gap with intention to achieve good light transmission. In order to make the best configuration fitting the current setup, photomultipliers (PMTs) are mounted on both ends of the detector system in the beam direction. This configuration causes long light paths inside the AC box, and therefore, the light loss by reflection and the Rayleigh scattering inside the aerogel radiator might become a significant problem. This leads to large dependence of decay positron detection efficiency on its incident angle and position.

There are three parameters to optimize the detector performance: (1) optimization of aerogel radiator thickness, (2) optimization of air-gap thickness, and (3) optimization of reflector structure. These optimizations have been done by the Monte Carlo simulation developed for the purpose of this AC counter design under the following conditions:

- The target radius is chosen to be 30 mm to increase the K^+ stopping efficiency and to reduce the probability of the bremsstrahlung creation in the stopper. Then, the distance from target center to the inner surface of the AC counter is decided to be 51 mm in order to put the AC counter as close as possible to the target system, as shown in Fig. 15.

- The kaons are generated under the assumption of originally designed J-PARC K1.1BR beamline parameters, so that horizontal and vertical beam profiles are taken into account. Therefore, the kaon stopping distribution is also included in the calculation.

- The positron momentum is assumed to be 247 MeV/c which corresponds to the e^+ momentum from the K_{e2} decay. The detection efficiency of the AC counter is calculated for decay positrons requiring the spectrometer transmission and the arrival at the C4 chamber.

- The refractive index of the aerogel radiator (n) should be less than 1.095 to reject 236 MeV/c muons from the $K_{\mu 2}$ decay. On the other hand, it is better to keep the largest n value because the aerogel radiator with larger n value produces more Cherenkov photons. Considering the availability of aerogel materials, we plan to use aerogel radiator with n of 1.08 in the P36 experiment.

- The Belle group successfully developed aerogel material with transmission length at the light wavelength of 400 nm as high as 40 mm or more at around n =1.045

[17]. It will be possible to make a $n = 1.08$ radiator with this long transmission length. In this simulation, it is assumed to be 40 mm.

- The Rayleigh scattering in the radiator and reflection at surfaces and mirrors are included into the calculation as light loss processes.

- Since a photomultiplier (PMT) with a quartz window is sensitive to the light wavelength between 160 nm to 650 nm, these photons are taken into account in the simulation. In general, the Cherenkov light intensity increases with decreasing wavelength. Therefore, Cherenkov photons in the short wavelength region are important to improve the detector performance.

From the above simulation calculation, we obtained the following parameters for the first prototype production. For the radiator thickness optimization, a thick aerogel radiator leads to a large number of Cherenkov photons, while suffers from large Rayleigh scattering. We concluded that the overall detection efficiency is maximized with a radiator thickness of 20 mm. For the air-gap thickness optimization, the efficiency dependence on the air-gap thickness is relatively small compared to that on the radiator thickness. It is found that a thicker air gap always introduces the higher detection efficiency. Therefore, the air gap is extended up to the inner radius of the beam hole in the CsI(Tl) barrel, as shown in Fig. 15. For the reflector optimization, we consider three cases such as a sawtooth mirror, a flat mirror, and a diffuse reflector. With a flat mirror, the overall detection efficiency is as low as 4.3%. On the contrary, the sawtooth structure optimized for the current simple configuration increases the efficiency as high as larger than 95%. The inefficiency of nearly 5% is turned out to be related to a bad light collection for the perpendicular e^+ incident on the detector.

5.2 Prototype Aerogel Cherenkov counter

In order to confirm the performance of the currently designed AC counter and the correctness of the simulation code, we constructed a prototype AC counter equipped with the sawtooth mirror.

Fig. 16 shows the trapezoidal one unit of the prototype AC counter. The sawtooth mirror has an acrylic base with an evaporation coating of aluminum and MgF_2 to enhance the reflection coefficient in the ultraviolet region. A Winston cone to focus the Cherenkov photons into the PMT entrance is also an acrylic base with an evaporation coating of aluminum and MgF_2. The other surface is an aluminum base with aluminized mylar. The PMT is chosen to be a Hamamatsu Photonics R2256-02 [18] which has a quartz window to transmit photons in the ultraviolet region.

Because we did not have enough time to develop new aerogel material for the first prototype production, we used a standard aerogel material with the refractive index n of 1.05 instead of 1.08 and a transmission length of 18 mm at 400 nm instead of 40 mm for this prototype counter. The smaller n decreases the Cherenkov photon yield and the small transmission length causes large Rayleigh scattering loss. This aerogel

material with the size of 110 mm × 110 mm × 10 mm was produced by Panasonic Electric Works Co. Ltd [19].

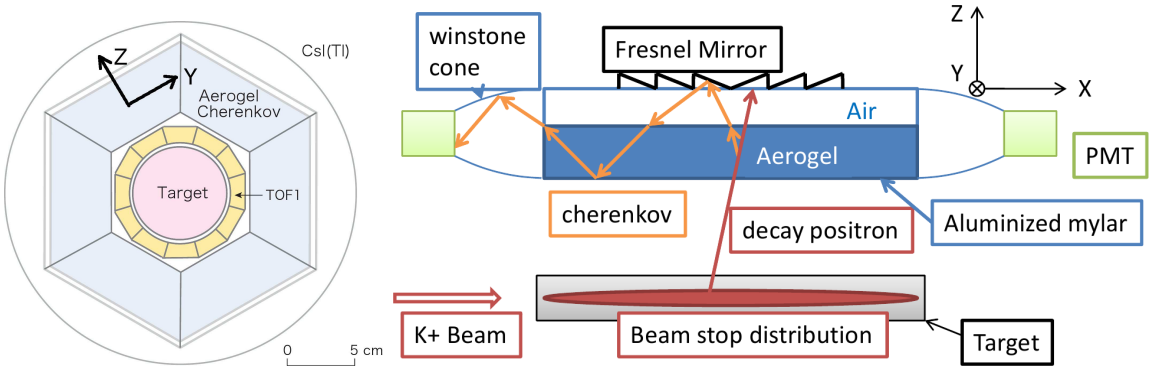

Figure 15: Schematic layout of the aerogel Cherenkov counter from the beam direction (left) and that from the side (right).

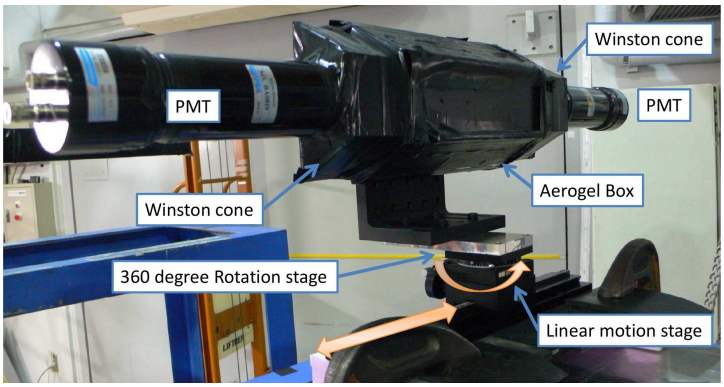

Figure 16: Prototype Aerogel Cherenkov counter (AC) (front view). The e^+ beam came from right side.

5.3 Test experiment of the prototype AC counter using a positron beam

5.3.1 Beam line and experimental setup

The AC test experiment was performed using an e^+ beam at the Research Center for Electron Photon Science (ELPH), Tohoku University. Instead of the e^+ momentum of 247 MeV/c, the e^+ beam momentum was employed to be 457 MeV/c, because the ELPH facility can serve higher beam intensity at this momentum. It is to be noted difference of beta factor between 457 MeV/c ($\beta = 0.999999$) and 247 MeV/c ($\beta = 0.999998$) does not cause any changes of the Cherenkov photon yield and angle at the 0.1% level.

As shown in Fig. 17, the prototype AC counter was installed between a fiber scintillator counter and a stop counter. This fiber scintillator was composed of 16 scintillation rods for the horizontal axis (HODO-X) and 16 for the vertical axis (HODO-Y). TDC and charge ADC data for each PMT were taken with a data trigger of (HODO-X OR) $\times$ (HODO-Y OR) $\times$ (STOP). Parallelism of the positron beam was good enough to confirm detector efficiency at the 0.1% level. Typical trigger rate was about 300 Hz. The AC counter was mounted on a 360 degree rotation stage to change the e^+ beam entrance angle to the AC counter. Moreover, this rotation stage was mounted on a linear motion stage to change the e^+ beam entrance position along the horizontal direction which corresponds to the K^+ beam axis in the P36 experiment. The AC counter tilt angle (TA) could be changed by adjusting an adapter attached to the backside of the AC counter.

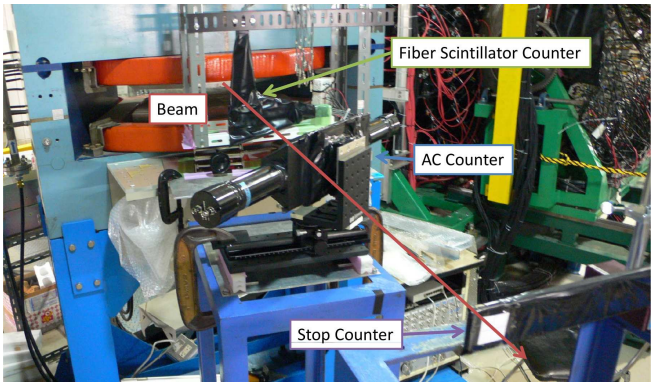

Figure 17: AC test experiment setup at ELPH

5.3.2 Data summary taken in the experiment

In the P36 experiment, the entrance position and angle of charged particles to the AC counter will be widely distributed. Therefore, in this test experiment, the performance of the prototype AC counter was studied by changing the e^+ beam entrance conditions to the counter. We took the data in the following conditions: (a) use of the sawtooth mirror with $TA = 0°$ (b) no use of the sawtooth mirror with $TA = 0°$, (c) use of the sawtooth mirror with $TA = 25.2°$. Each data set was composed of 9 combinations of the horizontal position and the horizontal rotation angle, as shown in Table 5. Also, calibration data set such as different positron momentum, pedestal run, different PMT gain, etc were taken.

5.3.3 Discussion for preliminarily results of the test experiment

The e^+ beam with 12 mm $\times$ 12 mm square shape was injected into the AC counter with the position and angle combinations, as shown in Table 5. The detection efficiency was simply computed with the condition that at least one of the two PMTs

Table 5: Combination of horizontal position and horizontal angle in the AC test experiment. The central position is defined to be 0.0 mm, and the right-hand side of Fig. 17 corresponds to positive positions. The angle perpendicular to the beam axis is defined to be 0 degree, and the right-hand side of figure 17 corresponds to positive rotation.

Data number	1	2	3	4	5	6	7	8	9
Angle (degree)	0.0	0.0	0.0	−44.4	44.4	44.4	63.0	63.0	63.0
Position (mm)	0.0	−50.0	−100.0	−71.4	0.0	35.7	0.0	22.7	45.4

detected one or more photons. For this computation, the optimized cut conditions to the ADC and TDC values were required for each data set. We successfully determined the experimental efficiency with an accuracy of 0.5% or better, as shown in Fig. 18 for the data with the sawtooth mirror. Here, the data for $TA = 0$ is only analyzed, and the $TA = 25^\circ$ data are yet to be analyzed. It should be emphasized that the high efficiency of nearly 100% was successfully attained for the finite angle incidents. On the other hand, for the 0 degree incident, the efficiency decreased as was expected qualitatively from the simulation. However, we did not find a drastic decrease of the efficiency for the zero-degree incident as in the simulation, seemingly due to the light diffusion in the radiator. The lack of the overall efficiency, which is obviously larger than 5%, can be attributed to the following points:

1. A standard aerogel material with the refractive index n of 1.05 instead of 1.08 and the transmission length of 18 mm instead of 40 mm at 400 nm was used in the prototype AC production.

2. To fit the aerogel into the AC counter box, we had to cut the aerogel material with a water-jet cutter. However, the surface condition of the cut materials was not good, which introduces an additional diffusing reflection at the surface.

3. Thickness of the cut aerogel piece was only 10 mm, thus we needed 22 pieces in the longitudinal direction inside the AC box. Reflection at the surface between each aerogel piece seriously disturbs the Cherenkov light direction.

Now, a new Monte Carlo simulation is going on taking into account these effects in order to reproduce the experimental data. For the second prototype, we certainly improve the detector performance by using a monolithic aerogel material with the index of $n = 1.08$ and the transmission length of 40 mm. Also, we have to solve the problem of the low efficiency at the zero-degree e^+ incident by improving the sawtooth mirror structure. By setting an additional diffuse reflector near the both ends of the aerogel material, the detailed sawtooth mirror structure will be conceivably optimized. From this mirror optimization and the adoption of the necessary improvements for the aerogel radiator, we will be able to suppress the overall inefficiency to far less than 5%. Since we already confirmed the efficiency of nearly 100% for the finite angle of the e^+ entrance, even for $n = 1.05$ and the transmission length of 18 mm, the realization of the AC counter with high ($\sim 100\%$) total efficiency will be quite feasible.

Figure 18: Preliminarily results of the test experiment. The AC efficiency is determined by changing the e^+ entrance conditions.

6 Summary

In this report, we presented the investigations on the P36 proposal, since it has been submitted. The systematic uncertainties in the R_K measurement were carefully estimated by grouping them into three categories: (1) imperfect reproducibility of the experimental conditions by a Monte Carlo simulation, (2) performance of particle identification, and (3) background contamination. The systematic uncertainty is obtained by adding each item in quadrature to be $\Delta R_K/R_K = 0.13\%$. In the heavy neutrino search, the experimental sensitivity of the $K^+ \to \mu^+ N$ decay was reconfirmed to be $\mathrm{Br}(K^+ \to \mu^+ N) \sim 10^{-8}$. A correct muon polarization form was given, with which the found signal can be confirmed. We successfully observed sufficiently high quality beam in the K1.1BR beamline test and concluded that we can carry out the P36 experiment at J-PARC. The test experiment for an aerogel Cherenkov counter was carried out and a good performance as an e^+ trigger was observed. In addition to the AC development which we presented in this report, we also made progress in the CsI(Tl) readout based on an avalanche photodiode with a current amplifier. The test experiment to study the energy resolution, timing resolution, and rate capability was performed. The results meet requirements for the P36 experiment. Regarding the budget request for the detector construction, we are continuing efforts to apply for Grand-in-Aids Research Support money. For the moment, we are concentrating on the detector parts relevant to P36 experiment, by postponing the construction of the muon polarimeter for TREK experiment.

Thus, we are making steady progress for the realization and preparation for the P36 experiment at J-PARC. Now, we would like to proceed to a more advanced stage by obtaining approval for this experiment.

Acknowledgement

We are indebted to Prof. T. Asaka for valuable discussion about the νMSM model, in particular the muon polarization calculation. We would like to thank Prof. Y. Okada for comments concerning to MSSM and νMSM.

References

[1] E. Goudzovski et al., arXiv:[hep-ex/1008.1219] (2010); E. Goudzovski et al., in proceedings of KAON09, PoS (KAON09) 025.

[2] F. Ambrosino et al., Eur. Phys. J. C64 (2009) 627; Erratum-ibid. C65 (2010) 703.

[3] S. Shimizu et al., Phys. Lett. **B495** (2000) 33.

[4] K. Horie et al., Phys. Lett. **B513** (2001) 311.

[5] M.A. Aliev et al., Phys. Lett.**B554** (2003) 7; M.A. Aliev et al., Eur. Phys. J. **46** (2006) 61.

[6] S. Shimizu et al., Phys. Rev. **D70** (2004) 037101.

[7] S. Shimizu et al., Phys. Lett. **B633** (2006) 190.

[8] J. Bijnens, G. Colangelo, G. Ecker, J. Gasser, arXiv:hep-ph/ 9411311. Published in 2nd DAPHNE Physics Handbook:315-389

[9] C.H. Chen, C.Q. Geng, C.C. Lih, Phys. Rev. D 77, 014004 (2008)

[10] C. Gatti, Eur. Phys. J. **C45** (2006) 417.

[11] S. Weinberg, Phys. Rev. **140**, 516 (1965)

[12] TREK homepage, http://trek.kek.jp/

[13] An 800 MeV/c separated kaon beam at J-PARC, J. Doornbos, April 2005.

[14] Addendum : An 800 MeV/c separated kaon beam at J-PARC, J. Doornbos, May 2007.

[15] J. Doornbos et al.; Optics design and performance of LESB3, a two-stage separated 800-MeV/c kaon beamline, Nucl.Instr. and Methods in Physics research **A444** (2000) 546.

[16] A. Yamamoto, KEK Report No.81-13, Study of Low Energy Intense Kaon Beam

[17] I. Adachi et al., Nuclear Instruments and Methods in Physics Research **A595** (2008) 180-182.

[18] Hamamatsu photonics K.K., http://sales.hamamatsu.com/index.php?id=13189298.

[19] Panasonic Electric Works Co. Ltd., http://panasonic-electric-works.net/